Gaussian distribution of inhomogeneous nickel–vanadium Schottky interface on silicon (100)

S Soltani[1,2] (ID)**, P M Gammon**[3]**, A Pérez-Tomas**[4]**, A Ferhat Hamida**[1,2] (ID) **and Y Terchi**[1] (ID)

[1] Department of Electronics, Faculty of technology Ferhat Abbas Setif1 University, Setif 19000, Algeria
[2] Optoelectronics and Component Laboratory, Ferhat Abbas Setif1 University, Setif 19000, Algeria
[3] School of Engineering, University of Warwick, Coventry CV4 7AL, United Kingdom
[4] IMB-CNM-CSIC, Campus UAB, Barcelona 08193, Spain

E-mail: soltanimicro@gmail.com

CrossMark

Abstract

This study presents the characterization of the nickel–vanadium (NiV) Schottky diode on n-type silicon (Si) in the temperature range 75 K–300 K. The experimental current–voltage (I–V) measurements are first analyzed by using the thermionic emission (TE) theory. For this purpose, the vertical optimization method is used to find the values of the TE parameters, i.e. the values of the ideality factor, barrier height, and series resistance. It is found that these parameters exhibit strong temperature dependence, i.e. an increase of the ideality factor and a decrease of the barrier height ϕ_B and the series resistance R_s when the temperature decreases, which is due to inhomogeneities at the Schottky interface. Therefore, we employ Werner's model under the assumption of a Gaussian distribution to analyze the temperature dependence of the TE parameters. The mean and standard deviation of the barrier height are obtained as $\phi_{B0} = 0.68$ eV and $\sigma_0 = 53.665$, respectively. In addition, we show that the apparent barrier height and apparent ideality factor are in accordance with Werner's model. Furthermore, we use the modified Richardson plot to find the value of the Richardson constant. The obtained value of the latter is $A^* = 111.56$ A cm^{-2} K^{-2} and is very close to the theoretical value of 112 A cm^{-2} K^{-2} of n-type Si. Finally, we investigate the temperature dependence of the ideality factor and show the validity of the T0-effect for the NiV/Si Schottky diode.

Keywords: I–V characteristics, metal–semiconductor interface, inhomogeneity, nickel–vanadium/silicon, vertical optimization method

(Some figures may appear in colour only in the online journal)

1. Introduction

Semiconductors have very important properties that have been deeply studied, exploited, developed, and applied in the fields of microelectronics and communication. The advance that has been achieved in the development of semiconductors is the outcome of understanding the physics that connects various of their aspects, such as their physical properties, manufacturing, structure, and characterization. The key to semiconductor physics is the band theory that summarizes the charge transport processes within these materials. It is well-known that

by putting a semiconductor in contact with a metal, a potential barrier is established at the interface. Depending on the nature of the used materials, the obtained component may be an ohmic contact or rectifier [1, 2]. From its discovery in 1874 to the present day, the metal-semiconductor contact, which is often called the Schottky diode, has been the subject of a great deal of research.

The established potential barrier at the metal–semiconductor interface has long been assumed homogeneous, i.e. constant over the entire surface [3]. Nevertheless, the homogeneous model includes various anomalies without

any physical explanation [4–6]. Particularly, the decrease in the barrier potential, the increase of the ideality factor when the temperature decreases, and the obtained Richardson constant value A^* that is less than the theoretical value $A^*_{th} = 112 \, A\,cm^{-2} \, K^{-2}$ for silicon [7]. Early in the 1970s, these anomalies were attributed to interface inhomogeneities [8], which are related to various reasons. For instance, the barrier height inhomogeneity is due to non-uniform metal thickness, interface layer composition, grain boundaries, etc [9]. Other sources of the interfacial inhomogeneities can include the reaction between the metal and the semiconductor, manufacturing faults, processing remnants (dirt, contamination), native oxide, uneven doping profiles, and crystal defects [4, 5, 10–12]. Although several models have been proposed in the literature to describe these inhomogeneities, only two among them, namely Werner [4] and Tung [5, 13] models, have been able to explain the majority of anomalies. In Tung's model [5], the barrier at a metal–semiconductor interface consists of locally non-uniform but interacting patches of different barrier heights embedded in a background of uniform barrier height. Moreover, the interaction of the high barrier and low barrier is described with the help of the so-called 'saddle point'. On the other hand, in Werner's model [4], the high barrier is assumed to be distributed according to a Gaussian distribution, which usually leads to an apparent barrier height that is both temperature and bias dependent. Despite their conceptual differences, both Tung's and Werner's models have been successfully used in the interpretation of experimental results on various metal-semiconductor Schottky contacts. Indeed, several studies have been performed using Werner's model to investigate Schottky diodes [14–30], whereas other researchers have been alternatively following Tung's model to explain inhomogeneous Schottky barrier heights [19, 30–45].

Nickel–vanadium (NiV) materials have various applications in the semiconductor industry [46]. Although both nickel (Ni) and vanadium (V) Schottky contacts with n-type Si have been fabricated and characterized separately in [47] and [48], respectively, Gammon *et al* [35] have been the first to study the NiV/Si Schottky contact. Nevertheless, the study performed in [35] consists only of studying the temperature-related nonlinearity at the NiV/Si interface. Moreover, Tung's model has been used in [35] and various flaws have been observed in the model. Indeed, the authors in [35] have reported a low accuracy of Tung's model at the lowest temperatures, which is due to the divergence at low temperatures of the two current paths built into Tung's model. To the best of our knowledge, there is no existing work that has reported the electrical transport characteristics of NiV/n-Si Schottky diode. This motivates us to study the current transport characteristics of NiV/Si Schottky diodes in a wide temperature range of 75 K–300 K.

In this paper, we characterize the NiV/Si Schottky diode on n-type silicon (Si) in the temperature range of 75 K–300 K. In order to obtain the values of the series resistance, barrier height, and ideality factor, we employ the thermionic emission (TE) theory and the vertical optimization method (VOM). Subsequently, we use Werner's model under the assumption of a Gaussian distribution of the barrier height to analyze the temperature dependence of the obtained values. For this purpose,

we extract the values of various parameters that characterize the NiV/Si Schottky diode, such as the mean $\bar{\phi}_B$ and the standard deviation σ of the barrier height, as well as the voltage coefficients ρ_2 and ρ_3. Moreover, by means of the modified Richardson plot, and by using the obtained values of $\bar{\phi}_B$ and σ, we determine the corrected value of the Richardson constant. Finally, we investigate the temperature dependence of the ideality factor and show the validity of the T0 effect.

2. Experimental details

Full details on the fabrication procedure were published in [35]. In brief, however, NiV Schottky diodes were fabricated on n-type silicon (100) substrates. The substrate comprised of a highly n-doped (100) Si substrate ($1.2 \times 10^{19} \, cm^{-3}$) and a 2 μm lightly phosphorous doped epitaxial layer ($1 \times 10^{16} \, cm^{-3}$). The pseudo-vertical diodes were fabricated by first cleaning the surfaces with a standard RCA clean, followed by a 3 μm CF4-plasma etch in a Sentech Etchlab 200 Reactive Ion Etcher to create a mesa structure that exposed the highly doped substrate. A common Ti cathode contact was then sputtered onto the exposed and roughened highly doped surface using a Mantis QPrep Deposition System, before being annealed in a Heatpulse 610 rapid thermal annealing system for 30 s at 800 °C in argon ambient. NiV was then sputtered onto the mesa surface to form the anode contact. After wire bonding, the devices were characterized using a fully automated closed-cycle-cryostat test setup, which took current–voltage (I–V) measurements between 75 K and 300 K at 25 K intervals.

3. Results and discussion

3.1. Current–voltage characteristics

The electrical forward current–voltage (I–V) measurements are analyzed using the standard TE theory. According to the latter, the theoretical I–V relation for a metal—semiconductor interface is given by [1, 2]

$$I = I_s \left[\exp \left(\frac{\beta}{n} \left(V - R_s I \right) \right) - 1 \right] \qquad (1)$$

with the saturation current I_s defined by

$$I_s = AA^* T^2 \exp \left(-\beta \phi_B \right) \qquad (2)$$

where $\beta = q/kT$ is the inverse thermal voltage, q is the elementary electric charge, k is the Boltzmann constant, T is the temperature, R_s is the series resistance of the diode, V is the applied voltage, n is the ideality factor, A is the diode area, A^* is the effective Richardson constant, and ϕ_B is the barrier height.

The obtained experimental I–V curves of the NiV/Si diode are shown in figure 1 for various values of the temperature. Our objective then is to find the values of the parameters in equation (1) that best fit the experimental I–V data, i.e. find the values of the ideality factor n, the saturation current I_s, and
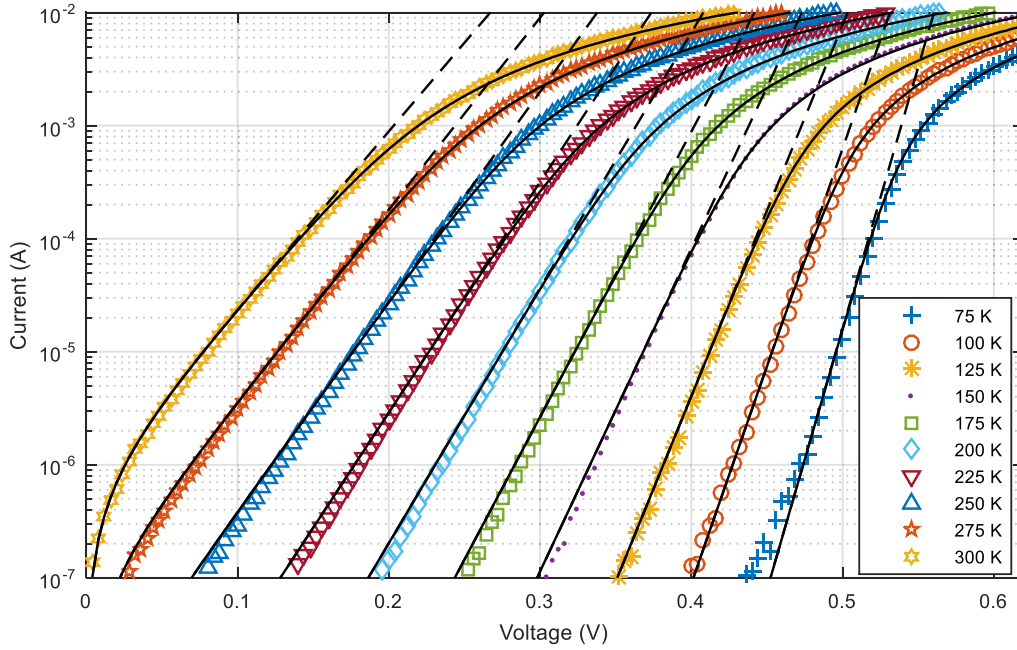
Figure 1. The experimental and fitted (*I–V*) plots at different temperatures. The dashed lines represent the linear fitting of the standard method and the solid lines represent the fitting by using the VOM.

the series resistance R_s. The barrier height can then be found by using equation (2) and the theoretical value of Richardson constant $A_{th}^* = 112\,\mathrm{A\,cm^{-2}\,K^{-2}}$ of n-type Si [7]. A simple approach that can be used to perform this task is the standard method, which neglects the series resistance and deduces, respectively, n and I_s from the slope and intercept of the linear region of the $\ln(I)$ vs. V curve. The linear fitting of the standard method for the case of the NiV/Si diode is shown in figure 1 (dashed lines). As can be seen from this figure, at each temperature, the linear fitting is only valid for a portion of the *I–V* curve, which is due to the existence of non-zero series resistance. For the purpose of finding the values of n, I_s, and R_s that best fit the *I–V* data in all regions, we use the VOM [49, 50]. Let $\hat{I}_k$ and $\hat{V}_k$ be the kth measured current and voltage at a given temperature T, respectively, and I_k be the corresponding theoretical current obtained by setting $V = \hat{V}_k$ in equation (1). The VOM seeks to find the values of the parameters n, I_s, and R_s that minimize the cost function given by

$$S = \sum_{k=1}^{N} \left(\frac{I_k - \hat{I}_k}{I_k} \right)^2 \tag{3}$$

with N being the total number of measurements. Therefore, the values of n, I_s, and R_s can be obtained by solving the system of equations given by

$$\begin{cases} \frac{\partial s}{\partial n} = 2 \sum_{N}^{k=1} \left(\frac{I_k - \hat{I}_k}{I_k^3} \right) \hat{I}_k \frac{\partial I_k}{\partial n} = 0 \\ \frac{\partial s}{\partial I_s} = 2 \sum_{N}^{k=1} \left(\frac{I_k - \hat{I}_k}{I_k^3} \right) \hat{I}_k \frac{\partial I_k}{\partial I_s} = 0 \quad , \\ \frac{\partial s}{\partial R_s} = 2 \sum_{N}^{k=1} \left(\frac{I_k - \hat{I}_k}{I_k^3} \right) \hat{I}_k \frac{\partial I_k}{\partial R_s} = 0 \end{cases} \tag{4}$$

which we have solved by using Newton–Raphson's method [50, 51]. The obtained results of n, ϕ_B, I_s and R_s for various values of the temperature, are shown in figure 2. Moreover, the theoretical *I–V* curves obtained from equation (1) with the corresponding values of the parameters obtained by the VOM are shown in figure 1 (solid lines). It is evident from figure 1 that the experimental and theoretical results exhibit excellent agreement. Furthermore, it can be seen from the results in figure 2 that, as the temperature increases, the values of the barrier height and the series resistance increase (from $\phi_B = 0.461$ eV and $R_s = 15.188\,\Omega$ at $T = 75$ K to $\phi_B = 0.624$ eV and $R_s = 16.145\,\Omega$ at $T = 300$ K), whereas the value of the ideality factor decreases (from $n = 1.453$ at $T = 75$ K to $n = 1.07$ at $T = 300$ K).

In figure 3, the experimental reverse bias *I–V* curves are shown for the temperature range 250 K–300 K. It should be noted, however, that the reverse bias *I–V* curves for temperatures lower than 250 K are not shown here due to the smallness of their reverse bias current values, which are lower than the precision of our measuring equipment, and thus very noisy and unreliable. From the reverse bias curves shown in figure 3, the value of the reverse saturation current is obtained as 3.32×10^{-9}, 4.48×10^{-8}, and 5×10^{-7} A for the temperature values of 250 K, 275 K, and 300 K, respectively. These values are very close to their corresponding values obtained from the forward bias curves as can be seen from figure 2(b). From these results and those of the saturation current shown in figure 2(b), it is evident that the saturation current decreases with decreasing temperatures, which is in accordance with the TE theory prediction. Furthermore, the reverse bias *I–V* curves in figure 3 and their forward counterparts in figure 1 demonstrate clearly that the NiV/Si Schottky diode has a very good forward-to-reverse (rectification) current ratio. For instance, at
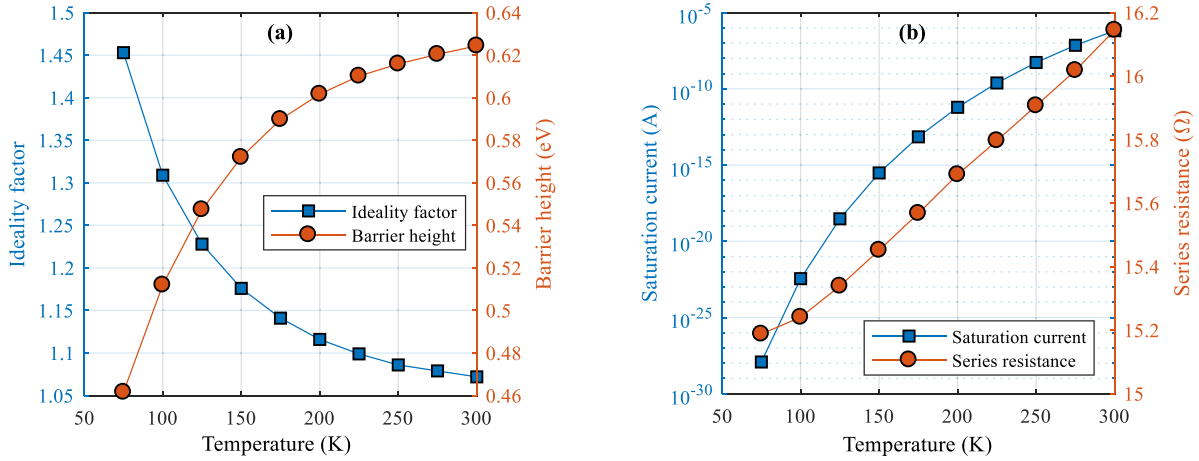
3

Figure 2. The obtained values of the parameters of the NiV/Si Schottky diode as functions of the temperature. (a) Ideality factor and barrier height. (b) Saturation current and series resistance.
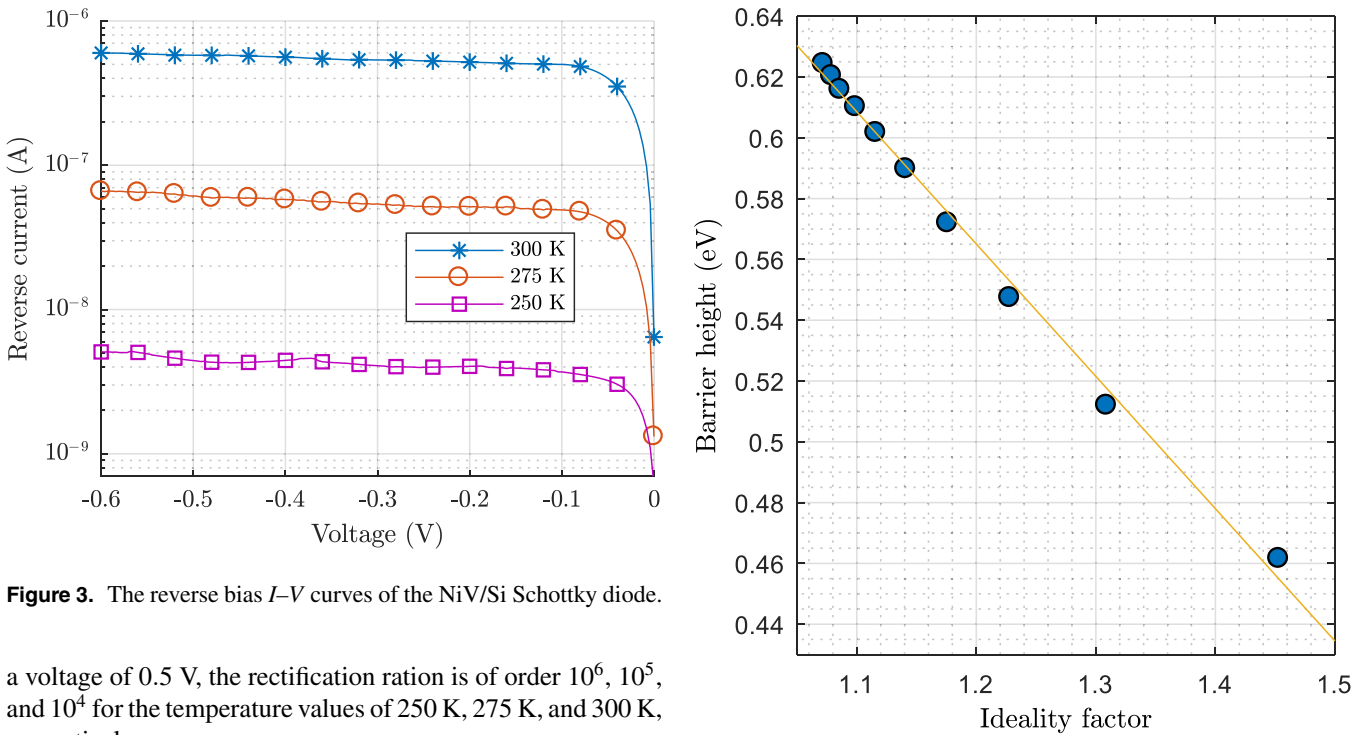

Figure 3. The reverse bias *I–V* curves of the NiV/Si Schottky diode.

a voltage of 0.5 V, the rectification ration is of order 10^6, 10^5, and 10^4 for the temperature values of 250 K, 275 K, and 300 K, respectively.

The temperature dependence of the ideality factor and the barrier height that are reported above are due to the inhomogeneities of the Schottky barrier. Indeed, the linear relation between the barrier height and ideality factor is demonstrated in figure 4 and it is a signature of inhomogeneities [5, 52, 53].

3.2. Inhomogeneous barrier analysis

As mentioned earlier in the introduction section, the inhomogeneities of the Schottky barrier can be explained by using Werner's model under the assumption of a Gaussian distribution of the barrier height. The probability density function of the barrier height is given by

$$P(\phi_{\mathrm{B}}) = \frac{1}{\sqrt{2\pi\sigma^2}} \exp\left(-\frac{\left(\phi_{\mathrm{B}} - \bar{\phi}_{\mathrm{B}}\right)^2}{2\sigma^2}\right) \quad (5)$$

Figure 4. The relation between the barrier height and the ideality factor.

where ϕ_{B}, $\bar{\phi}_{\mathrm{B}}$, and σ are the barrier height, its mean, and its standard deviation, respectively. Furthermore, a linear bias of $\bar{\phi}_{\mathrm{B}}$ and quadratic bias dependence of σ are assumed in Werner's model, i.e.

$$\bar{\phi}_{\mathrm{B}} - \bar{\phi}_{\mathrm{B0}} = \rho_2 V, \quad (6)$$

and

$$\sigma^2 - \sigma_0^2 = \rho_3 V \quad (7)$$

where ρ_2 and ρ_3 are coefficients that are temperature independent. Hence, the total current across the Schottky contact can be
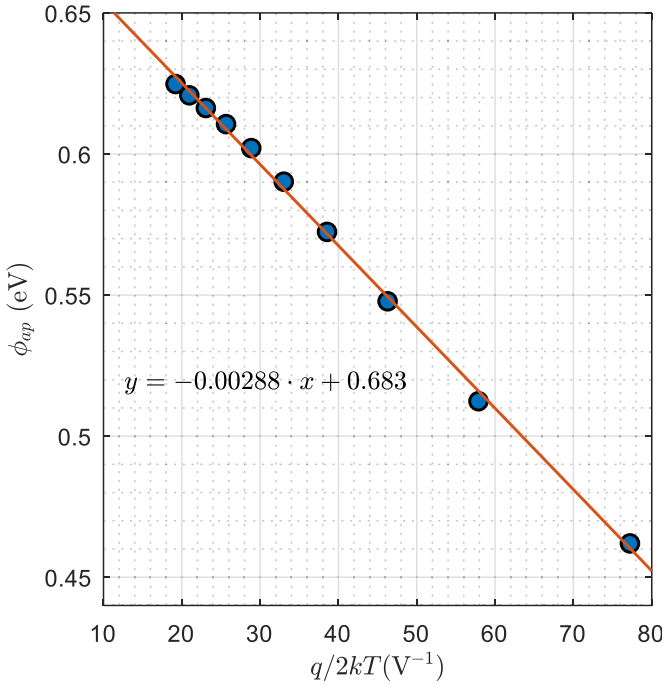
4
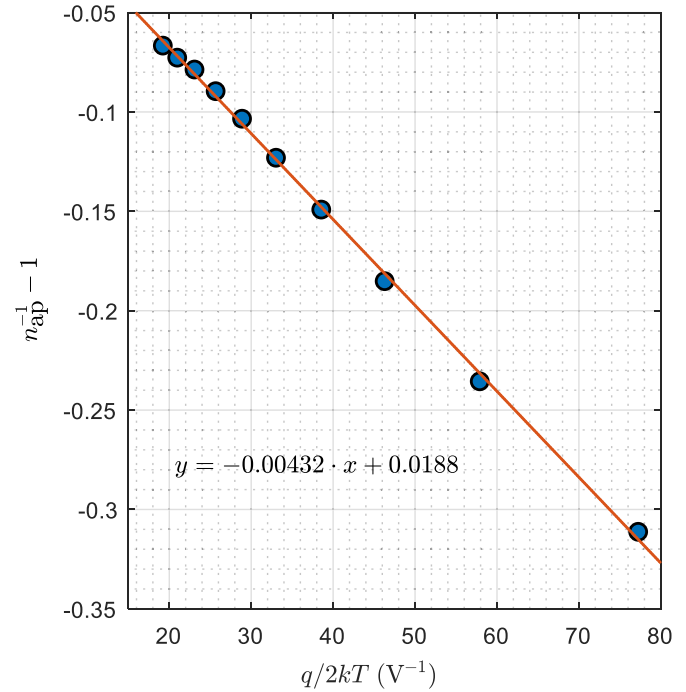
Figure 5. The apparent barrier height ϕ_{ap} versus $q/2kT$.

Figure 6. The $(n_{ap}^{-1} - 1)$ versus $q/2kT$ curve of the NiV/Si Schottky diode according to the Gaussian distribution.

obtained as

$$I = \int_{-\infty}^{\infty} i\left(\phi_{\mathrm{B}}, V\right) P\left(\phi_{\mathrm{B}}\right) \, \mathrm{d}\phi_{\mathrm{B}} \tag{8}$$

with $i\left(\phi_{\mathrm{B}}, V\right)$ being the current at a given barrier height ϕ_{B} and voltage V. By substituting $i\left(\phi_{\mathrm{B}}, V\right)$ and $P\left(\phi_{\mathrm{B}}\right)$ from equations (1) and (5), respectively, equation (8) yields

$$I = I_0 \left[\exp\left(\frac{\beta}{n_{\mathrm{ap}}} \left(V - R_{\mathrm{s}} I\right) \right) - 1 \right] \tag{9}$$

where

$$I_0 = AA^* T^2 \exp\left(-\beta \phi_{\mathrm{ap}}\right), \tag{10}$$

n_{ap} and ϕ_{ap} are, respectively, the apparent barrier height and the apparent ideality factor, which are given in Werner's model [4, 22, 23, 54] by

$$\phi_{\mathrm{ap}} = \bar{\phi}_{\mathrm{B}0} - \frac{\beta \sigma_0^2}{2} \tag{11}$$

and

$$\frac{1}{n_{\mathrm{ap}}} = 1 - \rho_2 + \frac{\beta \rho_3}{2}. \tag{12}$$

According to equation (11), the plot of ϕ_{ap} versus $q/2kT$ should be a straight line. The plot of ϕ_{ap} versus $q/2kT$ for the NiV/Si diode is given in in figure 5. As shown in this figure, the results are in good agreement with equation (11), and thus the values $\bar{\phi}_{\mathrm{B}0} = 0.68$ eV and $\sigma_0 = 53.665$ mV are obtained from this plot. Figure 6 shows the $(n_{\mathrm{ap}}^{-1} - 1)$ versus

$q/2kT$ plot of the NiV/Si diode. As seen, the obtained results are in accordance with equation (12). Therefore, the values of the voltage coefficients ρ_2 and ρ_3 can be obtained, respectively, from the intercept and the slope of the curve in figure 6 as $\rho_2 = -0.0188$ and $\rho_3 = -4.322$ mV

3.3. Richardson and modified Richardson plots

The conventional Richardson plot of $\ln\left(I_{\mathrm{s}}/T^2\right) = \ln\left(AA^*\right) - \beta \phi_{\mathrm{B}}$ versus q/kT is usually used to determine the Richardson constant A^* and the barrier height ϕ_{B}. Figure 7 shows the conventional Richardson plot for the NiV/Si diode from which the values of the barrier height and the Richardson constant are obtained as $\phi_{\mathrm{B}} = 0.410$ eV and $A^* = 3.072 \times 10^{-3}$ A cm^{-2} K^{-2}, respectively. However, the obtained value of the Richardson constant is much smaller than the theoretical value of 112 A cm^{-2} K^{-2} of n-type Si [7]. The small value of the Richardson constant suggests that the effective area is much smaller than the diode area [18]. Moreover, it is apparent from figure 7 that the conventional Richardson plot deviates from linearity, which is due to the inhomogeneity of the barrier height [54, 55]. This anomalous behavior can be explained by taking into account the inhomogeneity of the barrier height, which can be achieved by combining equation (10) and equation (11) as

$$\ln\left(\frac{I_0}{T^2}\right) - \frac{\beta^2 \sigma^2}{2} = \ln\left(AA^*\right) - \beta \bar{\phi}_{\mathrm{B}0}. \tag{13}$$

The modified Richardson plot of $\ln(I_0/T^2) - \beta^2 \sigma^2/2$ versus q/kT for the NiV/Si Schottky diode according to equation (13) is shown in figure 8. As seen, the plot is
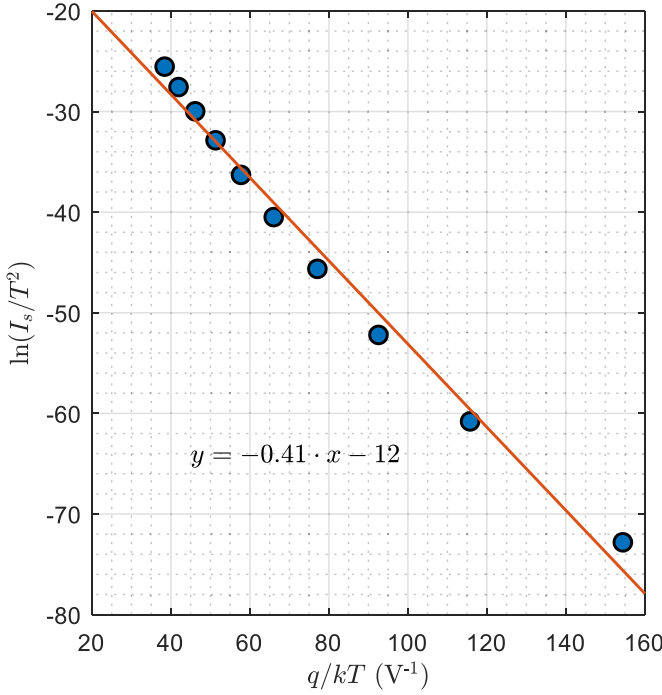
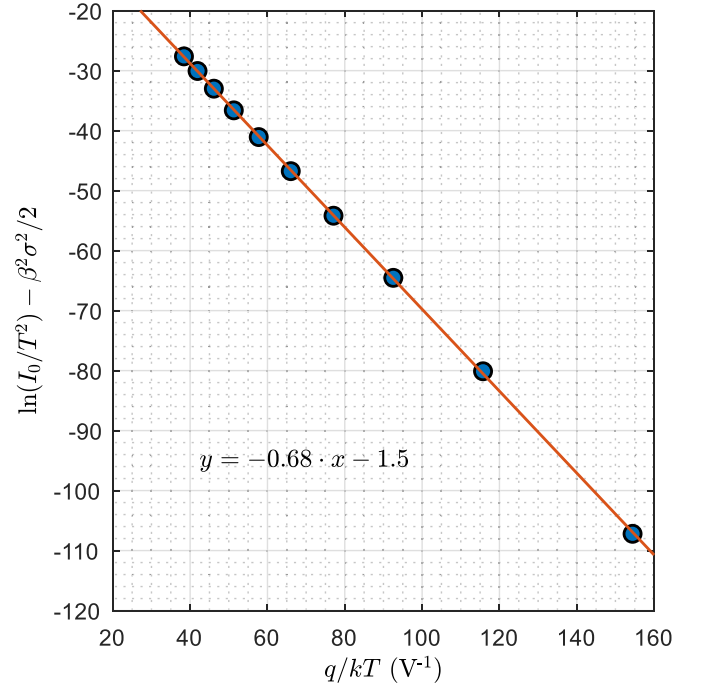**Figure 7.** The conventional Richardson plot for the NiV/Si Schottky diode.

Figure 8. The modified Richardson plot for the NiV/Si Schottky diode.

well-fitted by a straight line that gives $\bar{\phi}_{B0} = 0.68$ eV and $A^* = 111.56$ A cm^{-2} K^{-2} from the intercept and slope, respectively. The obtained value of $\bar{\phi}_{B0}$ matches perfectly the previously calculated mean barrier height that has been obtained from the plot of figure 5 (see section 3.2). Furthermore, the obtained value of the Richardson constant is very close to the theoretical value of 112 A cm^{-2} K^{-2} of n-type Si. These results clearly indicate the usefulness and validity of the modified Richardson plot.

3.4. T0 effect

The variation of the ideality factor with temperature in Schottky diodes is known as the T0 effect, or alternatively, as the T0 anomaly [18, 56]. According to Saxena [57], the temperature dependence of the ideality factor is usually given by

$$n(T) = 1 + \frac{T_0}{T} \tag{14}$$

where T_0 is a positive constant that is referred to as the excess temperature. On the other hand, according to Werner, the temperature dependence of the ideality factor can be obtained from equation (15) as

$$n(T) = \frac{1}{1 - \rho_2 + \frac{q\rho_3}{2kT}}. \tag{15}$$

In the case of $|\rho_2| \ll |q\rho_3/2kT| \ll 1$, which is valid for most cases of Schottky diodes [23], $n(T)$ in equation (15) can be approximated as [23]

$$n(T) \approx 1 - \frac{q\rho_3}{2kT}, \tag{16}$$

which is of the same form as equation (14). Therefore, by comparing equation (14) and equation (16), a theoretical approximation of T_0 can be obtained as

$$T_0 \approx -\frac{q\rho_3}{2k}. \tag{17}$$

By using the calculated value of $\rho_3 = -4.322$ mV, we obtain from equation (17), $T_0 \approx 25.07$ K. Figure 9 shows the experimental nT versus T plot together with its linear fitting and illustrates the temperature dependence of the ideality factor for the NiV/Si Schottky diode. In the same figure, the nT versus T plot corresponding to equation (16) with the calculated value of T_0 is shown as well. As can be seen from figure 9, equation (16) well approximates the temperature dependence of the ideality factor. Nevertheless, it is evident that, in contrast to equation (16), the slope of the experimental data deviates slightly from unity. Such deviation of the slope has been observed in various Schottky diodes [23] and it is mainly due to the temperature dependence of T0 [49, 56]. In addition, equation (16) is derived from an approximation that may not always be accurate [56]. Indeed, in our case, the condition of $|q\rho_3/2kT| \ll 1$ is weakly valid in the considered temperature range. Therefore, as has been reported in several works [18, 23, 56, 58, 59], the temperature dependence of the ideality factor, in this case, is given by

$$n(T) = n_0 + \frac{\tilde{T}_0}{T} \tag{18}$$

with n_0 and $\tilde{T}_0$ can be obtained for the NiV/Si diode from the slope and intercept of the linear fitting of the experimental nT versus T plot as $n_0 = 0.95$ and $\tilde{T}_0 = 36$ K. As demonstrated in
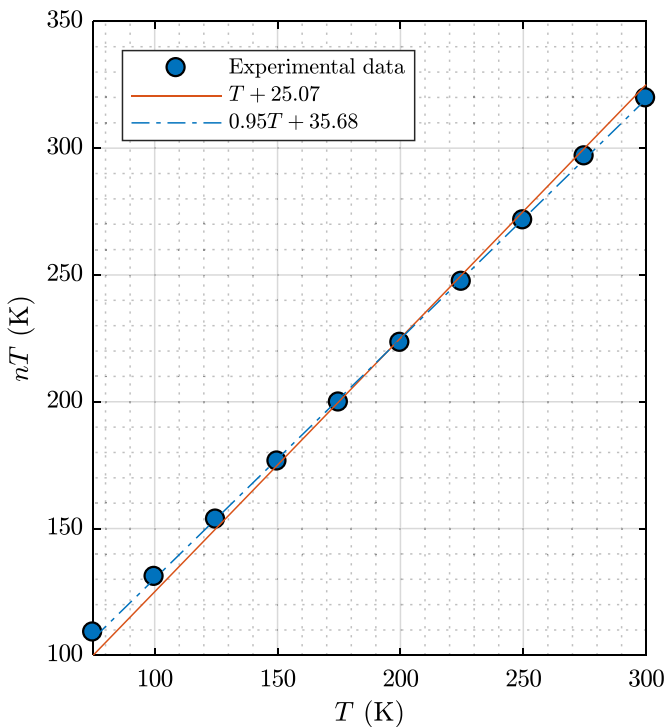
Figure 9. Plot of nT versus T for the NiV/Si Schottky diode indicating the temperature dependence of the ideality factor.

figure 9, with the obtained values of n_0 and $\tilde{T}_0$, equation (18) describes the temperature dependence of the ideality factor more accurately than equation (16).

4. Conclusion

In this paper, the temperature dependence of the *I–V* characteristics of the NiV/Si Schottky diode has been reported in the 75 K–300 K temperature range. The *I–V* measurements have been analyzed by using the TE theory. For this purpose, the VOM has been used in order to find the values of the ideality factor, barrier height, and series resistance that best fit the experimental *I–V* measurements. It has been established that the ideality factor, barrier height, and series resistance vary, respectively, in the ranges of 1.07–1.453, 0.461–0.624 eV, and 15.188–16.145 Ω. Moreover, it has been observed that in contrast to the ideality factor, which decreases when the temperature increases, both the barrier height and series resistance increase when the temperature increases. This temperature dependence has been attributed to the inhomogeneities of the barrier height at the Schottky interface. Therefore, in order to consider these inhomogeneities, we have used Werner's model under the assumption of a Gaussian distribution of the barrier height. The mean and standard deviation of the barrier height have been obtained as $\phi_{B0} = 0.68$ eV and $\sigma_0 = 53.665$ mV, respectively. Moreover, the experimental results of the apparent ideality factor and barrier height have been found to fit well with Werner's model. Furthermore, by means of the modified Richardson plot of $\ln\left(I_s/T^2\right) - \beta^2\sigma^2/2$ versus q/kT, the value of the Richardson constant has been obtained

as $A^* = 111.56$ A cm^{-2} K^{-2}, which is very close to the theoretical value of 112 A cm^{-2} K^{-2} of n-type Si. Finally, the T0-effect has been investigated and it has been shown that the experimental results of the ideality factor fit well with the well-known equation $n = n_0 + \tilde{T}_0/T$ with $n_0 = 0.95$ and $\tilde{T}_0 = 36$ K.

ORCID iDs

S Soltani ⓘ https://orcid.org/0000-0002-8069-975X
A Ferhat Hamida ⓘ https://orcid.org/0000-0001-9992-0162
Y Terchi ⓘ https://orcid.org/0000-0002-8136-5890

References

[1] Rhoderick E H and Williams R H 1988 *Metal–Semiconductor Contacts* 2nd edn (Oxford: Clarendon) p 11
[2] Sze S M 1981 *Physics of Semiconductor Devices* (New York: Wiley-Interscience) p 154
[3] Bethe H A 1942 *MIT Rad. Lab. Rep.* **43** 12
[4] Werner J H and Gttler H H 1991 *J. Appl. Phys.* **69** 1522
[5] Tung R T 1992 *Phys. Rev.* B **45** 13509
[6] Sullivan J P, Tung R T, Pinto M R and Graham W R 1991 *J. Appl. Phys.* **70** 7403
[7] Andrews J M and Lepselter M P 1970 *Solid-State Electron.* **13** 1011
[8] Canali C, Catellani F, Mantovani S and Prudenziati M 1977 *J. Phys. D: Appl. Phys.* **10** 2481
[9] Singh R, Sharma P, Khan M A, Garg V, Awasth V, Keanti A and Mukherjee S 2016 *J. Phys. D: Appl. Phys.* **49** 445303
[10] Gammon P M *et al* 2013 *J. Appl. Phys.* **114** 223704
[11] Song Y P, Van. R L, Meirhaeghe W, Laflere H and Cardo F 1986 *Solid-State Electron.* **29** 633–8
[12] Aydın M E, Yıldırım N and Türüt A 2007 *J. Appl. Phys.* **102** 043701
[13] Tung R T 2001 *Mater. Sci. Eng.* R **35** 1
[14] Durmuş H and Karataş Ş 2018 *Int. J. Electron.* **106** 507
[15] Taşcıoğlu I, Aydemir U and Altındal Ş 2010 *J. Appl. Phys.* **108** 064506
[16] Somvanshi D and Jit S 2013 *IEEE Electron Device Lett.* **34** 1238–40
[17] Lin Y J and Lin J H 2014 *Appl. Surf. Sci.* **311** 224–9
[18] Boussouar L, Ouennoughi Z, Rouag N, Sellai A, Weiss R and Ryssel H 2011 *Microelectron. Eng.* **88** 969–75
[19] Shivaraman S, Herman L H, Rana F, Park J and Spencer M G 2012 *Appl. Phys. Lett.* **100** 183112
[20] Zhang T, Raynaud C and Planson D 2019 *Eur. Phys. J. Appl. Phys.* **85** 10102
[21] Tecimer H, Türüt A, Uslu H, Altındal Ş and Uslu İ 2013 *Sensors Actuators* A **199** 194–201
[22] Toumi S, Ferhat-Hamida A, Boussouar L, Sellai A, Ouennoughi Z and Ryssel H 2009 *Microelectron. Eng.* **86** 303–9
[23] Ouennoughi Z, Toumi S and Weiss R 2015 *Physica* B **456** 176–81
[24] Kumar A, Vinayak S and Singh R 2013 *Curr. Appl. Phys.* **13** 1137–42
[25] Jian G *et al* 2018 *AIP Adv.* **8** 015316
[26] Jin W, Mu X, Zhang K, Shanga Z and Dai L 2018 *Phys. Chem. Chem. Phys.* **20** 19932–7
[27] Jin W, Liu Y, Yuan K, Zhang K, Ye Y, Wei W and Dai L 2018 *IEEE Electron Device Lett.* **40** 119–22
[28] Moun M and Singh R 2018 *Semicond. Sci. Technol.* **33** 125001
[29] Park Y, Ahn K S and Kim H 2012 *Japan. J. Appl. Phys.* **51** 09MK01

[30] Shin J H, Park J, Jang S, Jang T and Kim K S 2013 *Appl. Phys. Lett.* **102** 243505

[31] Ru G P, Van Meirhaeghe R L, Forment S, Jiang Y L, Qu X P, Zhu S and Li B Z 2005 *Solid-State Electron.* **49** 606–11

[32] Tunç T, Altindal Ş, Uslu I, Dökme I and Uslu H 2011 *Mater. Sci. Semicond. Process.* **14** 139–45

[33] Janardhanam V, Park Y K, Ahn K S and Choi C J 2012 *J. Alloys Compd.* **534** 37–41

[34] Zeng J J and Lin Y J 2014 *Appl. Phys. Lett.* **104** 133506

[35] Gammon P M *et al* 2012 *J. Appl. Phys.* **112** 114513

[36] Omar S U, Sudarshan T S, Rana T A, Song H and Chandrashekhar M V S 2014 *J. Phys. D: Appl. Phys.* **47** 295102

[37] Dong S X, Bai Y, Tang Y D, Chen H, Tian X L, Yang C Y and Liu X Y 2018 *Chin. Phys.* B **27** 097305

[38] Brezeanu G, Pristavu G, Draghici F, Badila M and Pascu R 2017 *J. Appl. Phys.* **122** 084501

[39] Korucu D and Turut A 2014 *Int. J. Electron.* **101** 1595–606

[40] Ferhat Hamida A, Ouennoughi Z, Sellai A, Weiss R and Ryssel H 2008 *Semicond. Sci. Technol.* **23** 045005

[41] Cetin H and Ayyildiz E 2010 *Physica* B **405** 559–63

[42] Roccaforte F, Giannazzo F, Alberti A, Sper M, Cannas M, Cora I, Pecz B, Iucolano F and Greco G 2019 *Mater. Sci. Semicond. Process.* **94** 164–70

[43] Iucolano F, Roccaforte F, Giannazzo F and Raineri V 2007 *Appl. Phys. Lett.* **90** 092119

[44] Tripathi S K 2010 *J. Mater. Sci.* **45** 5468–71

[45] Hussain I, Soomro M Y, Bano N, Nur O and Willander M 2013 *J. Appl. Phys.* **113** 234509

[46] Guo W, Turner S and Cawley E 2004 *US Patent App. 10/720* p 231

[47] Nanda Kumar Reddy N, Ananda P, Verma V K and Rahim Bakash K 2019 *Surf. Rev. Lett.* **26** 1950073

[48] Kim J S, Choi H H, Son S H and Choi S Y 2001 *Appl. Phys. Lett.* **79** 860

[49] Toumi S and Ouennoughi Z 2019 *Indian J. Phys.* **93** 1155–62

[50] Toumi S, Ouennoughi Z, Strenger K C and Frey L 2016 *Solid-State Electron.* **122** 56

[51] Press W H, Teukolsky S A, Vetterling W T and Flannery B P 1992 *Nemerical Recipes in Fortran 77, the Art of Scientific Computing* Vol. 1 (Cambridge: Press Syndicate of the University of Cambridge) p 355

[52] Schmitsdorf R F, Kampen T U and Monch W 1995 *Surf. Sci.* **324** 249–56

[53] Schmitsdorf R F, Kampen T U and Mönch W 1997 *J. Vac. Sci. Technol.* B **15** 1221

[54] Chawanda A, Mtangi W, Auret F D, Nel J, Nyamhere C and Diale M 2012 *Physica* B **407** 1574–7

[55] Horvath Z J 1996 *Solid-State Electron.* **39** 176–8

[56] Aldemir D A, Kokce A and Ozdemir A F 2012 *Microelectron. Eng.* **98** 6–11

[57] Saxena A N 1969 *Surf. Sci.* **13** 151–71

[58] Djeghlouf A, Hamri D, Teffahi A, Saidane A, Al Mashary F S, Al Huwayz M M, Henini M, Orak I, Albadri A M and Alyamani A Y 2019 *J. Alloys Compd.* **775** 202–13

[59] Demirezen S and Altındal Ş 2010 *Curr. Appl. Phys.* **10** 1188–95